

Internal Vacillations in Stratosphere-Only Models

R. K. SCOTT* AND P. H. HAYNES

*Centre for Atmospheric Science, Department of Applied Mathematics and Theoretical Physics,
University of Cambridge, Cambridge, United Kingdom*

(Manuscript received 9 July 1998, in final form 24 June 1999)

ABSTRACT

An investigation is made of steady-state and vacillating regimes, in an idealized numerical model of the winter stratosphere, to improve understanding of possible mechanisms for variability in the real stratosphere. Variability obtained here is internal to the model in the sense that all external parameters are kept constant throughout the model integrations. The model used allows arbitrary height and latitude structure in waves and zonal-mean flow, so the investigation extends previous work on steady and vacillating regimes in channel models that include only a single mode to represent the latitudinal structure.

The variation of model behavior with two parameters, the “strength” of the radiative basic state and the amplitude of the lower-boundary wave forcing, is investigated. For each radiative state considered, two qualitatively different vacillating regimes and two different steady states are obtained for different values of wave forcing. The vacillating regimes are interpreted in terms of wave and mean flow diagnostics, and the controlling mechanisms are shown to depend upon the latitudinal degrees of freedom. The steady-state regimes are found to be both obtainable under identical external conditions, that is, the model exhibits multiple-flow equilibria. The property of multiple-flow equilibria is known to exist in the simpler height-only channel models, but appears not to have been found before in models with both height and latitude structure.

1. Introduction

This paper addresses aspects of the short-term variability of the extratropical winter stratosphere. Many previous studies have provided computational and observational evidence that such variability can arise through variability in the conditions external to the stratosphere, for example, in the tropospheric wave forcing. These studies have often been focused on stratospheric sudden warmings, a dramatic form of such variability in which strong polar westerlies undergo rapid wave-induced deceleration, even reversing to easterlies with the destruction of the polar vortex in the case of the major warming. The first mechanistic model of the sudden warming (Matsuno 1971) used an impulsive increase in tropospheric wave forcing to initiate wave-induced deceleration in the upper stratosphere and subsequent descent of a zero wind critical level. Many further numerical studies (see, e.g., Andrews et al. 1987, for an overview and for additional references) have ex-

tended the early work of Matsuno, continuing the idea that it is an increase in lower-boundary forcing that leads to the warming, although it is recognized that there may be considerable time delay between such an increase and the warming itself (e.g., Dunkerton et al. 1981).

Idealized numerical models have illustrated the alternative possibility that such variability can arise spontaneously under constant external conditions. The first such study was by Holton and Mass (1976), who used a quasigeostrophic, periodic β -channel model with height dependence to obtain vacillating solutions under constant wave forcing and thermal relaxation. These solutions were investigated in detail by Yoden (1987a,b), who also used the strength of the wave forcing, h_0 , as an external bifurcation parameter. He observed multiple-flow regimes existing for certain ranges of h_0 and bifurcations between steady and vacillating flow regimes at critical values of h_0 . The rapid deceleration obtained by Matsuno's sudden warming model was interpreted as a transition between steady and vacillating regimes induced by the impulsive increase in wave forcing. Yoden analyzed two distinct types of vacillations with different characteristics, obtained for moderate and large values of the wave forcing. Another approach was adopted by Chao (1985), who increased the wave forcing quasi-statically and found rapid, catastrophe-like transitions between flow regimes, without the need for the impulsive increase in wave forcing used

* Current affiliation: College of Oceanic and Atmospheric Sciences, Oregon State University, Corvallis, Oregon.

Corresponding author address: Dr. Peter H. Haynes, Dept. Applied Mathematics and Theoretical Physics, University of Cambridge, Silver Street, Cambridge, CB3 9EW United Kingdom.
E-mail: phh@damtp.cam.ac.uk

by Matsuno. See Yoden (1987a, Fig. 8) for an overview of how the different interpretations are related.

The highly idealized studies of Yoden and predecessors were limited by the absence of latitudinal structure since only a single cross-channel mode was retained. The present study extends this work by allowing a more general latitudinal structure as well as including spherical geometry. As before, the aim is to determine to what extent internal variability can arise, purely as a result of the intrinsic dynamics of the model, rather than as a consequence of transience in the external conditions. It is thus hoped to gain further insight into the mechanisms for variability in the real stratosphere, in particular whether events such as the stratospheric sudden warming are inherent features of the flow or whether they require transient forcing such as might arise from tropospheric variability. We see understanding of the model response to steady forcing as a prerequisite to an understanding of the response to more realistic, time-varying forcing. An illustration of the complexity of the response when the radiative basic state and the wave forcing are time varying was given in Scott (1996, chapter 3); see section 5 below for a short discussion of the implications of the steady forcing investigation presented here for behavior with seasonally varying forcing.

In the extension from one-dimensional, height only, to two-dimensional, height and latitude structure, properties of Rossby wave propagation and the mean flow response must be considered. In the 1D case, waves forced at the lower boundary are either evanescent or vertically propagating, according to the well-known Charney–Drazin criterion [Andrews et al. 1987, chapter 4, Eq. (4.5.15).] In the 2D case, waves will propagate in both height and latitude. Some guide to the direction of propagation may be obtained by considering the refractive index, n_s , given in the quasigeostrophic approximation by

$$n_s^2 = \frac{\bar{q}_\phi}{a(\bar{u} - c)} - \frac{s^2}{a^2 \cos^2 \phi} - \frac{f^2}{4N^2 H^2}, \quad (1)$$

(Matsuno 1970). Here c is the phase speed of the (linear) waves and $s = 1, 2, \dots$ is the zonal wavenumber. Under suitable scale-separation conditions, waves will tend to propagate upgradient of n_s^2 . Further, the latitudinal dependence of the n_s^2 implies that in the absence of mean flow variations there is a tendency for waves to propagate equatorward, such tendency being stronger for the higher wavenumbers (Karoly and Hoskins 1982).

It is important to determine when upward propagating waves can penetrate into higher latitudes, since it is in those regions that, due to the smaller moment of inertia of these regions, dissipation of the waves can most effectively alter the mean flow. Typically there will be enhanced wave propagation in regions of strong positive latitudinal gradients of isentropic potential vorticity and reduced wave propagation in regions where this gradient

is weak. This can be seen in the linear, quasigeostrophic case from Eq. (1). These strong gradients can themselves arise from the cumulative effects of breaking or dissipating waves eroding the polar vortex (e.g., McIntyre 1982 and references therein) and can be destroyed in the process of a sudden warming by the destruction of the polar vortex.

Another important aspect of the latitudinal structure with spherical geometry is the role of low latitudes in the extratropical evolution. Since waves tend to propagate equatorward, there will be a systematic effect on the mean flow at low latitudes. Because of the latitudinal variation in Coriolis parameter, the mean flow at low latitudes is less constrained by the radiative relaxation than at mid- and high latitudes (e.g., Holton et al. 1995; Haynes 1998; Scott and Haynes 1998). Further, there is evidence that the low-latitude mean flow structure will affect the propagation of waves in the extratropical stratosphere; studies include investigations between the relationship of the phase of the quasi-biennial oscillation and the occurrence of stratospheric sudden warmings (e.g., Holton and Tan 1982; O’Sullivan and Dunkerton 1994). This aspect will not play a significant role in the present study, however; the vacillations under consideration happen on a shorter timescale than the effective timescale of relaxation of low latitudes. On the other hand, the timescale for the model to reach a stable vacillating regime is in general quite long and could be related to the timescale required for low-latitude adjustment.

A mechanistic stratosphere-only model of the primitive equations, with spherical geometry and latitude–height structure, is used with constant external conditions. One zonal wavenumber is retained. The model is therefore of the “zonally truncated” type often used for sudden warming studies in the 1980s. The main advantage of using such a model in this study is the ability to perform long integrations to final steady or vacillating states for a large number of different external parameter values. Since the aim is to show how the addition of latitudinal structure allows different responses, such an approach can also be argued to be a logical extension of the earlier studies mentioned above. We present a detailed investigation only of the case when the longitudinal structure is wavenumber 1. Qualitatively similar results are found when the structure is wavenumber 2, albeit for different parameter values.

The amplitude of the lower-boundary wave forcing, h_0 , and the “strength” of the radiative basic state, defined below, are treated as external parameters that are different between model integrations. The dependence of the model responses on these external parameters is described in section 3. Essentially, there are two qualitatively different steady-state responses and two qualitatively different vacillating responses; typical responses are selected for further analysis. Additionally, a parameter range is found for which multiple-flow regimes, two steady states, exist under identical external condi-

tions, the selection of a particular steady state depending on the history of the model evolution. The multiple equilibria here correspond to those found by Yoden in the more restrictive Holton and Mass channel model, in which there is only one latitudinal degree of freedom. In section 4 the characteristics of the different responses are compared to those obtained by Yoden with the channel model, and some further details are noted. Conclusions are given in section 5.

2. Model description

The model used in this study is a mechanistic primitive equation model developed by Dr. Saravanan with pressure as the vertical coordinate and a spectral representation in the horizontal, using a hemispheric domain. The time stepping uses the semi-implicit scheme, treating terms associated with gravity waves implicitly, and uses a Robert time filter to damp the computational mode associated with the semi-implicit scheme (Haltiner and Williams 1980). There are 21 pressure levels, equally spaced in log-pressure, $z = -H \ln(p/p_s)$ where $p_s = 100\,000$ Pa, spanning $z_B = 11.9$ km (19 000 Pa) to $z_T = 88$ km (0.22 Pa), at intervals $\Delta z = 3.81$ km, and 21 latitudinal Legendre modes.¹ The reference temperature profile is that of an isothermal atmosphere with $T_{\text{ref}} = 240$ K, corresponding to a scale height, H , of 7 km. In the zonal direction only the zonal and wave-1 components are retained. The extent to which such severe truncation can represent the large-scale features of the nonlinear evolution is discussed in, for example, Haynes and McIntyre (1987) and references therein.

The lower-boundary wave forcing is through a perturbation in the geopotential height field near the lowest model level. This is of the form

$$\Phi' = h_0 E(t) G(\phi), \quad (2)$$

where $E(t)$ is grown smoothly from $E(t = 0) = 0$ to $E(t > t_s) = 1$, with $t_s = 100$ days and $E(0 < t < t_s) = \sin^2(\pi t/2t_s)$ in most cases. The latitudinal structure is given by $G(\phi) = 4\mu^2(1 - \mu^2)$, where $\mu = \sin\phi$. This has a maximum $G(\phi) = 1$ located at $\phi = 45^\circ$.

The radiative basic state, $\theta_r(\phi, z)$, is defined by a certain time within a notional seasonal cycle. This cycle is a time-varying sinusoidal superposition of summer and winter potential temperature fields, $\theta_{RS}(\phi, z)$ and $\theta_{RW}(\phi, z)$, given by $r\theta_{RS} + (1 - r)\theta_{RW}$ with $r(t) = (1 + \cos 2\pi t/T)/2$. Here t/T can be regarded as a (constant) external parameter, varied between integrations. Taking

$12t/T = 4, 4.5, 5, 6$, gives a radiative basic state corresponding to perpetual late October, early November, late November or late December with respect to this cycle. (Note that the basic state corresponding to late October also corresponds to late February, etc.) The potential temperature fields, θ_{RS} and θ_{RW} , are calculated from specified velocity profiles, U_{RS} and U_{RW} , by requiring thermal wind balance of the radiative basic state. The velocity fields are given by $U_{RS} = U_R(-\phi \geq 0)$ and $U_{RW} = U_R(\phi \geq 0)$, with

$$U_R(\phi, z) = \cos\phi \cos\left[\frac{\pi(z - z_B)}{2(z_T - z_B)}\right] \times [u_0 \tanh[b_0(\phi - \phi_0)] + J_1 + J_2 + J_3], \quad (3)$$

for constants u_0, b_0, ϕ_0 , and where the $J_i(\phi, z)$ are defined by

$$J_i = u_i \operatorname{sech}[b_i(\phi - \phi_i)] \operatorname{sech}[a_i(z - z_i)], \quad i = 1, 2, 3, \quad (4)$$

for constants $u_i, b_i, \phi_i, a_i, z_i$. The velocity field, U_R , given by Eq. (3) can therefore be regarded as a superposition of three jets, which we take to be a westerly midlatitude winter jet, an easterly midlatitude summer jet, and an easterly equatorial jet. The values of the constants are chosen accordingly to give a reasonable representation of a realistic state in radiative equilibrium; for this investigation they are

$$\begin{aligned} u_0 &= 20 \text{ m s}^{-1}, & b_0 &= 0.1, & \phi_0 &= 20^\circ, \\ u_1 &= 340 \text{ m s}^{-1}, & b_1 &= 0.04, & \phi_1 &= 60^\circ, \\ a_1 &= 0.05, & z_1 &= 65 \text{ km}, \\ u_2 &= -20 \text{ m s}^{-1}, & b_2 &= 0.1, & \phi_2 &= 15^\circ, \\ a_2 &= 0.3, & z_2 &= 30 \text{ km}, & \text{and} \\ u_3 &= -200 \text{ m s}^{-1}, & b_3 &= 0.03, & \phi_3 &= -55^\circ, \\ a_3 &= 0.08, & z_3 &= 70 \text{ km}. \end{aligned} \quad (5)$$

When balancing, the zonal mean geopotential at the lower boundary, as well as the interior temperature field, is determined by requiring that $\mathbf{T}^T \cdot \boldsymbol{\beta} \equiv 0$, where \mathbf{T} is a vector of temperatures at each pressure level, and $\boldsymbol{\beta}$ is a binomial vector of alternating sign. This is one way of ensuring that a two-grid wave in the temperature field is minimized and is a simple modification (for pressure coordinates) of the approach set out in Hoskins and Simmons (1975).

The radiative relaxation rate is given as a function of height by $\alpha(z) = \{1.5 + \tanh[(z - 35)/7]\} \times 10^{-6} \text{ s}^{-1}$, as in Holton (1976). Rayleigh friction is applied above $z = 50$ km, in a sponge layer, relaxing to a zero velocity field at rate $\kappa(z) = \{1.02 - \exp[(50 - z)/40]\} \times 5 \times 10^{-6} \text{ s}^{-1}$. Finally there is horizontal-scale selective damping using a ∇^8 hyperdiffusion with a damping rate

¹ This is equivalent to a latitudinal spacing of approximately 5.6° and was chosen to provide a reasonably well-resolved latitudinal structure. To check the sensitivity to latitudinal resolution, some of the runs were repeated with 31 latitudinal modes; quantitative differences were found in the values of wave forcing separating different regimes, but the qualitative behavior was the same.

TABLE 1. Different model responses for different parameter values of the radiative basic state (columns) and the lower-boundary wave forcing amplitude (rows). Two entries in a single box indicates that two distinct final flow regimes are obtainable under identical parameter values.

	60	70	80	90	100	110	120	140	160	180	200	240	280
D	s_0	s_0	s_0										
		s_1	s_1	v_2	v_2	v_2	i	i	v_3	v_3	v_3	v_3	—
N1	s_0	s_0	s_0	s_0									
		s_1	s_1	s_1	s_1	s_1	s_1	v_2	v_3	v_3	v_3	—	—
N0	s_0	s_0	s_0	s_0									
			s_1	s_1	s_1	v_2	v_2	v_2	v_3	v_3	—	—	—
O	s_0	s_0	s_0										
				s_1	s_1	v_2	v_2	v_3	—	—	—	—	—

of 4 day^{-1} at the smallest scales (highest total wavenumbers).

3. Results

Results are presented typically for model integrations of 1000 days, this usually being sufficient to determine the final dynamical regime for a particular forcing and radiative state. In some intermediate cases, where the model takes longer to reach such a regime, a continuation of a further 1000 or more days is used. Such long integrations allow consideration of the internal variability alone. In particular, they remove the transient behavior involved in adjusting the model from a zonally symmetric initial radiative state to a dynamic equilibrium with a time-averaged balance between wave forcing and radiative relaxation.

The parameter range investigated includes four radiative states, corresponding to late October (O), early November (N0), late November (N1), and late December (D). These are calculated as being 121, 136, 152, and 183 days after the the summer solstice with respect to the seasonal cycle outlined in section 2. The forcing amplitude, h_0 , is also varied as an external parameter from 60 to 300 m in steps of 10 or 20 m. The set of final model regimes obtained with this parameter range is summarized in Table 1. Qualitatively different regimes are obtained in different parameter regions. Two different steady-state regimes are denoted by s_0 and s_1 and two different vacillating regimes are denoted by v_2 and v_3 . An intermediate regime, i , is also obtained, characterized by intermittency between the two vacillating regimes v_2 and v_3 . Within each group, the final regimes exhibit qualitatively similar dynamical features and have a smooth dependence on the parameter values. All the results presented below were obtained using a wavenumber-1 longitudinal structure and wave forcing. However, similar behavior was found using wavenumber 2. In particular, the series D was repeated and steady and vacillating regimes were obtained, though for different values of the wave forcing parameter.

For certain parameter values both of the steady-state regimes are obtained. In these cases, the selection of a particular regime is determined by the history of the evolution. For the selection of s_0 , the wave forcing am-

plitude is grown over 100 days from 0 to its final value, h_0 , with $E(t)$ as described in section 2. It should be noted that the unforced steady states, those with $h_0 = 0$, belong to the class s_0 . For the selection of s_1 , on the other hand, the wave forcing amplitude is grown over 100 days from 0 to a value of 160 m (also with a sine squared time evolution) and then decreased linearly over the next 300 days to its final value h_0 . The stronger forcing in the early stages of the integration takes the model state dynamically far from s_0 and the subsequent decrease to h_0 results in a different final regime of s_1 .

Latitude–height cross sections of zonal velocity are shown in Fig. 1 for typical cases of the different final regimes s_0 , s_1 , v_2 , and v_3 , obtained with radiative state N1 and wave forcing $h_0 = 80$ (s_0 and s_1), $h_0 = 140$ (v_2), and $h_0 = 200$ (v_3). The vacillating regimes have been time averaged over several periods. In addition to the markedly different time-average structures of v_2 and v_3 the cycles themselves are qualitatively different (the reader may wish to refer ahead to Figs. 12a,c for an extended time series of each of v_2 and v_3). Further, as h_0 increases beyond a critical value between 140 and 200 there is sharp change in the nature of the vacillating response. In contrast, there is a strong similarity between the regimes s_1 and v_2 , which is stronger still for values of h_0 closer to the transition between the two states. On the other hand, s_1 differs considerably from s_0 , even though the final external forcing conditions (the final values of h_0) are identical between these two integrations. The interpretation is that s_0 lies on a different solution branch from s_1 and v_2 , whereas s_1 and v_2 are on the same branch and separated by a bifurcation point, $h_c \approx 130$ m, with respect to the parameter h_0 . It is not clear what is the precise nature of the bifurcation. There is complicated dependence of the response on h_0 over a very narrow range of h_0 . This will be discussed more fully in sections 3 and 4b below. Similar behavior is observed with the other radiative states, O, N0, and D, except that no multiple steady states are observed in O.

The transition from v_2 to v_3 is quite different in nature. With the radiative state D and wave forcing $h_0 = 120$ and $h_0 = 140$ integrations were continued to 10 000 days. The results showed intermittency between the two vacillating regimes, v_2 and v_3 , with [D, $h_0 = 120$] finally reaching a sustained v_2 response after 5000 days and

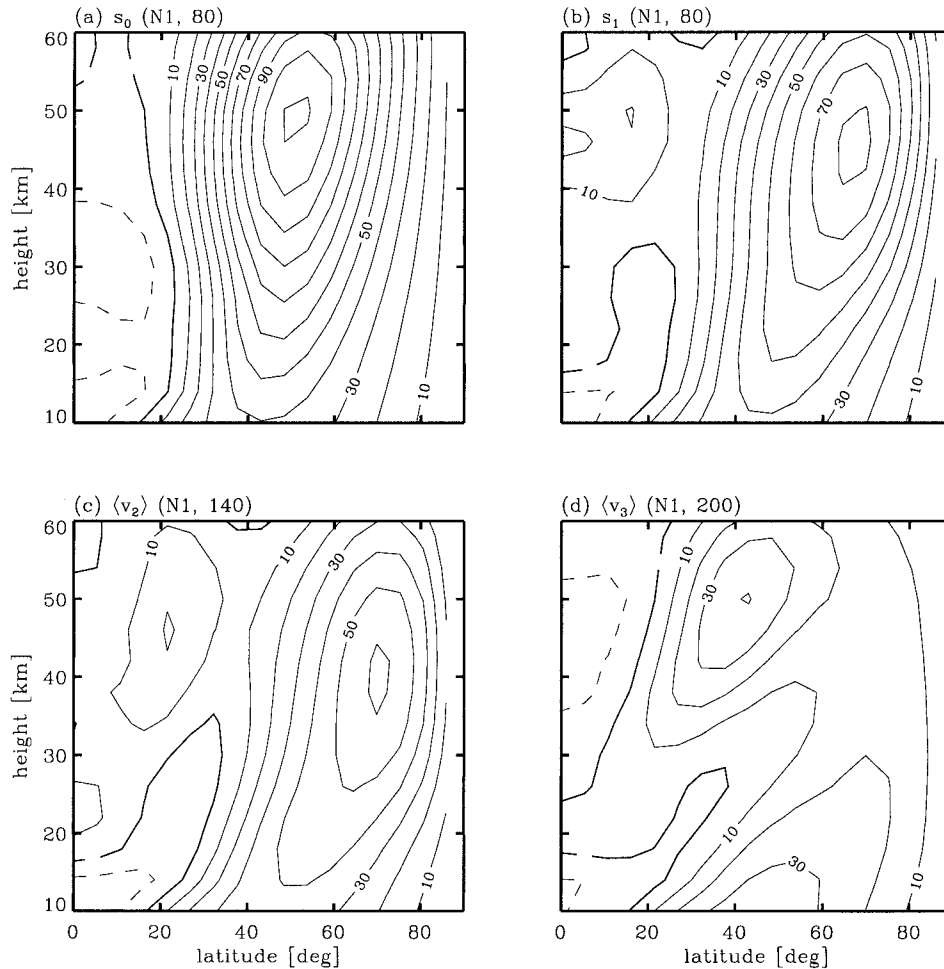
Zonal velocity for s_0 , s_1 , $\langle v_2 \rangle$, $\langle v_3 \rangle$ 

FIG. 1. Height–latitude cross section of zonal mean zonal velocity for two steady-state and two vacillation regimes obtained with radiative basic state N1, corresponding to late Nov, for various wave-forcing amplitudes, h_0 : (a) steady state s_0 , $h_0 = 80$ m; (b) steady state s_1 , $h_0 = 80$ m; (c) vacillation v_2 , $h_0 = 140$ m; (d) vacillation v_3 , $h_0 = 200$ m. Note that (a) and (b) are obtained under identical external (forcing) conditions, but that the approach to steady state is along different solution branches. Also note that (c) and (d) have been averaged over several vacillation cycles. Contour interval is 10 m s^{-1} , solid lines are positive, dashed lines are negative, and thick lines are zero.

[D, $h_0 = 140$] showing periods of both v_2 and v_3 right out to 10 000 days. The intermittency is characterized typically by long intervals (~ 500 days) resembling v_2 , but with less distinct periodicity, that separate shorter intervals (~ 200 days) resembling v_3 . With the radiative state N1, the transition from v_2 to v_3 is more sudden with respect to increasing h_0 : for $h_0 = 145$ the final state v_2 is reached quickly; for $h_0 = 150$ the final state v_3 is reached only after 1000 days, before which time v_2 is the dominant signal. A statistical analysis of much longer integrations and with intermediate forcing values might yield further insight. See section 4b below for further details.

The period of the vacillating regime v_3 has a clear dependence on the wave forcing, h_0 ; the period decreases as h_0 increases. For the case of strong radiative

state, D, the average period decreases from 110 days with $h_0 = 160$ to 42 days with $h_0 = 260$. In contrast, there is relatively little variation of the period of v_2 , which is 64 days for [D, $h_0 = 100$], and 95 days for [N1, $h_0 = 140$]. Beyond v_3 in all cases the wave forcing is so large that the zonal mean velocity field is permanently held far from the radiative state (denoted by a dash in Table 1). There is still substantial variability in this regime but it does not appear relevant to winter stratospheric processes on account of the absence of a realistic polar vortex. In the cases of stronger radiative state the onset of this regime occurs at larger h_0 as expected.

Before proceeding to a diagnostic description of the four different final regimes, it is interesting to note that the steady state, s_1 , here stable in a hemispheric domain,

is unstable to hemispherically asymmetric disturbances. The instability gives rise to yet another different class of vacillating solutions, v_1 , with the same time-averaged zonal mean structure as s_1 . The period of v_1 is approximately 20 days, significantly shorter than either of v_2 or v_3 , and the amplitude of the vacillation, measured by the zonal velocity at, say, 60° latitude and 38-km height, is also smaller than that of v_2 or v_3 . Diagnostic details of v_1 were discussed in Scott (1996), where this solution arose from latitudinally symmetric initial, boundary, and forcing conditions and where an asymmetric disturbance was introduced by numerical round-off errors in the spectral transform routines. The nature of the vacillation is summarized in section 4c below. In the current investigation, the model evolution is maintained as latitudinally symmetric by including only the relevant Legendre polynomials. Since v_1 is not present under this latitudinal symmetry, it is not included in the description given in Table 1.

A diagnostic description is now given for each of the four final regimes illustrated in Fig. 1. As examples, integrations are studied with parameter values the same as those in the figure, namely, N1, $h_0 = 80$ (s_0); N1, $h_0 = 80$ (s_1); N1, $h_0 = 140$ (v_2); N1, $h_0 = 200$ (v_3).

a. Steady state s_0

Integrating the model with no wave forcing, that is, $h_0 = 0$, yields a final steady state slightly different from the radiative equilibrium state on account of the competing effects of Rayleigh friction and the ∇^8 hyperdiffusion. This unforced steady state belongs to the class of steady states s_0 obtained for relatively small forcing amplitudes, in that the velocity structure obtained for $h_0 > 0$ exhibits only small departures from the unforced

steady state. Departures are shown in Fig. 2 for the cases $h_0 = 60$ and $h_0 = 80$. It is seen that increasing the forcing increases the strength of the low-latitude velocity deficit, an increase in forcing of 10 m resulting in a decrease in velocity of about 5 m s^{-1} . Attending the low-latitude deficit there is a smaller increase in velocity in midlatitudes. The pattern suggests that increasing the forcing results in more wave activity propagating to mid- and low latitudes. It resembles, though is weaker than, the midlatitude vortex erosion typical before a sudden warming, studied, for example, by Dunkerton et al. (1981). At the small wave-forcing amplitudes in this regime, however, no such sudden warming takes place. Instead, the waves remain “defocused,” propagating to low latitudes and dissipating.

The defocusing can be seen more clearly in the Eliassen–Palm (E–P) cross section shown in Fig. 3a. The waves forced at the lower boundary are deviated sharply equatorward between 10 and 20 km. There is a region of strong E–P flux convergence at low latitudes, coinciding with the region of weak zonal velocities (Fig. 1a). Thus, the region of weak velocities appears to behave as a partially absorbing critical layer. Figure 3a also shows that not all the wave activity is absorbed; there is some upward and poleward propagation out of the region, consistent with partial reflection, but the predominant direction of propagation again turns equatorward higher in the stratosphere.

The effect on the potential vorticity (PV) distribution, specifically the latitudinal gradient of PV on isentropes, is shown in Fig. 3b. This has been rescaled in the vertical by a factor of $(\theta/\theta_0)^{-9/2}$, where θ is potential temperature and $\theta_0 = 420 \text{ K}$ is a reference constant, following Lait (1994), to remove the exponential vertical dependence and enable plotting in the height–latitude plane. Fol-

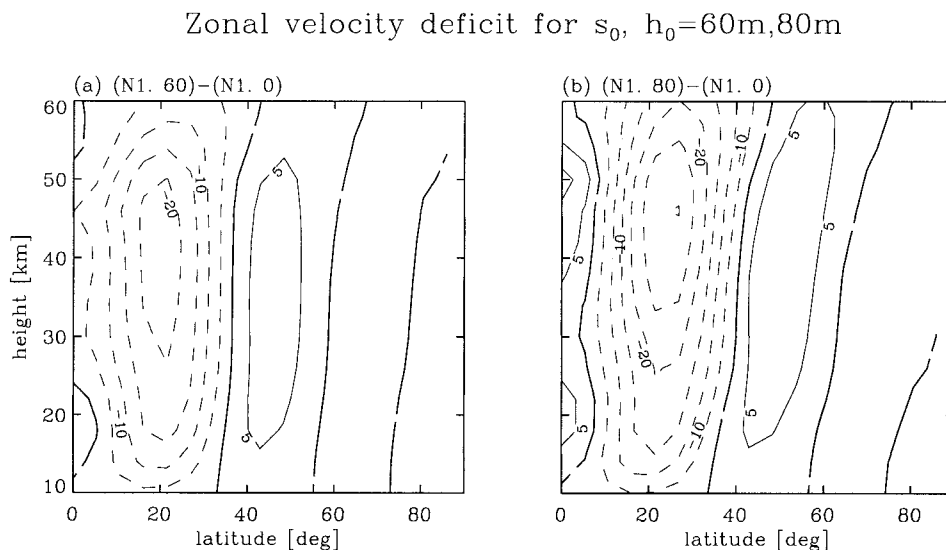


FIG. 2. Height–latitude cross section of zonal mean zonal velocity difference for steady states s_0 with various wave-forcing amplitude: (a) $[N1, h_0 = 60]$ minus $[N1, h_0 = 0]$; (b) $[N1, h_0 = 80]$ minus $[N1, h_0 = 0]$. Contour interval is 5 m s^{-1} .

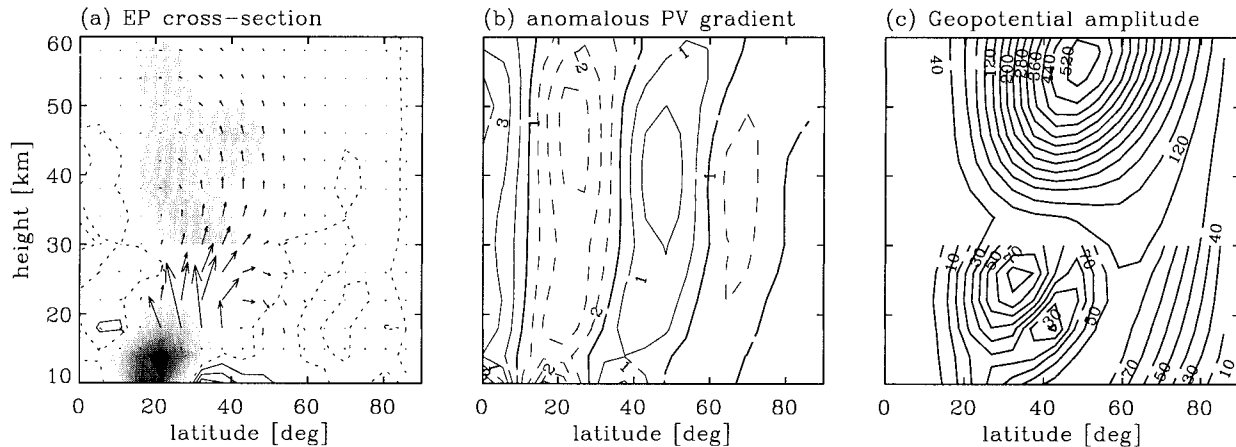
Steady state s_0 , (N1, 80)

FIG. 3. Steady state s_0 obtained with radiative state N1 and wave forcing $h_0 = 80$. Height–latitude cross sections of (a) E–P flux and divergence, with the graphical conventions of Dunkerton et al. (1981), contour and shading interval is 0.2 below 30 km and 0.04 above 30 km, in units of $2\pi a^3 \rho_e \times 10^{-7} \text{ m s}^{-2}$, negative values (convergence) are shaded and zero contour is dotted; (b) latitudinal PV gradient minus the latitudinal PV gradient of the unforced state [N1, $h_0 = 0$], contour interval is $10^{-5} \text{ K kg}^{-1} \text{ m}^2 \text{ s}^{-1}$; (c) wave-1 geopotential height amplitude, contour interval is 10 m below 30 km and 40 m above 30 km.

lowing the rescaling, the latitudinal gradient at constant potential temperature was calculated. The PV gradient, rather than the PV itself, is shown since it is the gradient that gives the clearest indication of regions favorable to wave propagation. Finally the difference between the forced and the unforced steady states was taken, as in Fig. 2 above. The figure shows that the result of the wave forcing is a weakening of PV gradients in low latitudes, where there is wave dissipation, together with a strengthening of PV gradients in midlatitudes. Analysis of the longitudinal structure revealed a closing of contours of PV on isentropes, and only a small correlation between eddy meridional velocity and eddy PV, $\overline{v'q'}$, similar (in the limited, single-wavenumber framework) to that expected from a critical layer that had reached a state of partial reflection (e.g., Haynes and McIntyre 1987). The longitudinal structure showed little variation with height, but was stronger in the lower- and upper-stratosphere, weaker in the middle, matching the regions of E–P flux convergence.

The geopotential height amplitudes are also in agreement with the above picture. Typically there is a tendency for larger geopotential amplitudes to exist in regions of stronger zonal velocity (Simmons 1974). However, Fig. 3c shows a local geopotential amplitude maximum at 25 km, 30°, occurring where there is no similar maximum in the zonal velocity and which therefore is associated with larger wave activity. On the other hand, the local geopotential amplitude minimum at 20 km, 40°, is associated with lower wave activity. The pattern is consistent with wave reflection from the critical-layer region; that is, the effective source of wave activity is equatorward, rather than poleward of the wave activity maximum.

b. Steady state s_1

For wave forcing amplitudes larger than $h_0 = 95$ (for the N1 case) the s_0 steady-state regime is absent and the model response lies on a different solution branch. On this branch, the s_1 steady-state regime is obtained with forcing amplitudes in the range $70 \leq h_0 \leq 120$. Where the s_1 branch overlaps the s_0 branch, s_1 is obtained by perturbing the response far from s_0 by temporarily larger forcing amplitudes (see section 3, paragraph 2). Figure 1a,b shows the different zonal velocity fields of s_0 and s_1 for identical external parameters (N1, $h_0 = 80$). The main differences are weaker low- and midlatitude velocities and a weaker but tighter, more poleward vortex in s_1 . Considering departures in the zonal velocity of s_1 , between the case with $h_0 = 70$ and cases with larger h_0 , reveals further differences from s_0 . Now the main departures of the zonal velocity for increasing h_0 occur in midlatitudes and are larger than before, an increase in h_0 of 10 m now results in a decrease in velocity typically of 5–10 m s^{-1} at 50° with larger decreases in velocity at lower forcing amplitudes and smaller decreases at higher amplitudes.

The same diagnostics shown for s_0 in Fig. 3 are shown in Fig. 4 for comparison. There is now a much larger E–P flux into midlatitudes than before, with significant flux convergence also in midlatitudes. (Note that the flux arrows have been rescaled by a factor of 5, i.e., a similar length arrow now denotes five times the flux of before.) Consequently the effect of the waves on the PV field is different; Fig. 4b shows that the midlatitude PV gradients have been considerably reduced from the values of the unforced steady state. On the other hand, the high-latitude PV gradients, poleward of 65°, have been

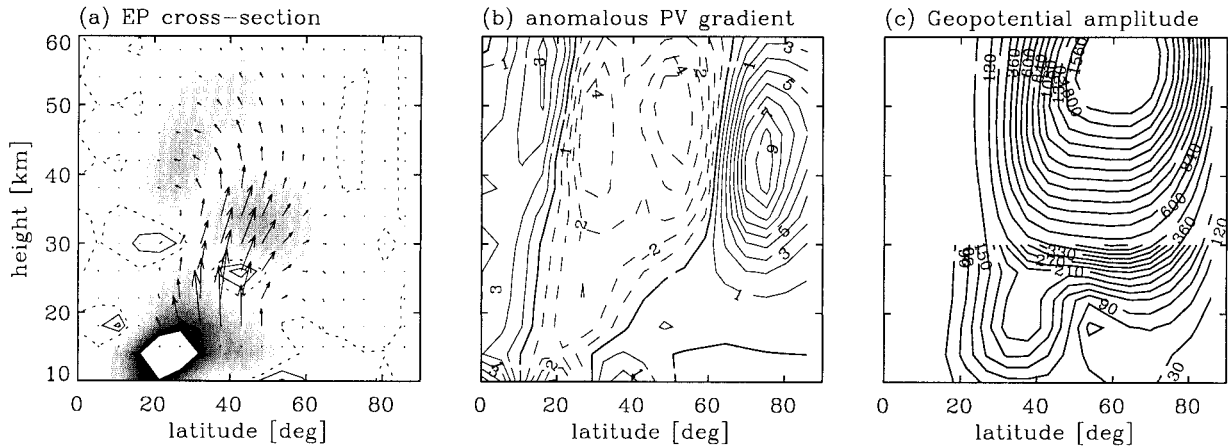
Steady state s_1 , (N1, 80)

FIG. 4. Steady state s_1 obtained with radiative state N1 and wave forcing $h_0 = 80$ and with temporarily stronger initial forcing. As Fig. 3 except s_1 instead of s_0 and (a) unit arrows represent 5 times the flux of Fig. 3 and contour interval is now 0.2 at all heights (in the same units); (b) no change; (c) contour interval is now 30 m below 30 km and 120 m above 30 km.

considerably increased. Geopotential amplitudes are also larger throughout the whole stratosphere, despite weaker zonal velocities. Though the s_1 vortex is tighter and confined to higher latitudes, showing more similarity to a preconditioned vortex before a sudden warming than the s_0 vortex, even so the wave amplitudes are still insufficient to cause further preconditioning and to trigger a sudden warming.

c. Vacillation v_2

When the wave forcing, h_0 , is increased beyond $h_0 = 130$ (for N1), the steady-state solution s_1 is replaced by a vacillating solution, v_2 . The present method of finding steady states, that is, by integrating until a steady state is reached, does not indicate whether the transition is due to s_1 losing stability in a Hopf-type bifurcation or whether s_1 actually disappears. However, some details are revealed in the transition between s_1 and v_2 by looking at smaller forcing increments. The interval $130 < h_0 < 135$ is apparently a region of parameter space in which the behavior is chaotic, characterized by small, irregular fluctuations about a mean state that is close to s_1 . Considering zonal mean velocity variations at 60° latitude and 42-km height the maximum changes are typically from around 60 to around 20 m s^{-1} or vice versa over a time interval of around 40 days. These maximum swings are separated by longer intervals during which smaller variations are observed. At $h_0 = 135$ these irregular fluctuations give way to much smaller regular vacillations, with a zonal velocity at 60° latitude and 42-km height that remains between 36.5 and 38.1 m s^{-1} . As h_0 is increased further these small-amplitude vacillations give way to the new class of vacillations, v_2 . Although larger in amplitude, the form of the v_2

vacillation remains that of a gentle undulation, rather than a series of sudden warmings.

The time evolution of zonal mean velocity, geopotential height amplitude, and zonal mean potential vorticity over a typical vacillation cycle (taken from days 870–970 of N1 with $h_0 = 140$, relabelled as days 0–100) is shown in Fig. 5. The cycle comprises a gradual strengthening of the mid- to upper-stratospheric polar vortex over days 10–40, followed by a gradual weakening of the vortex over days 60–100. In the lower stratosphere there is relatively little variation over the cycle. The strengthening and weakening can be understood in terms of wave dissipation rearranging the PV distribution in the mid–upper stratosphere, Fig. 5c. In the early stage, Fig. 6a shows weak E–P flux convergence in mid- to low latitudes. Associated with this is a small equatorward flux of PV also in mid- to low latitudes, shown around day 20 by decreasing PV at 40° and increasing PV at 20° . At higher latitudes, where the convergence is weaker, the evolution of the vortex is dominated by radiative relaxation, acting here on a time-scale of approximately 5 days, and the vortex strengthens. In the late stage, Fig. 6c shows stronger E–P flux in mid- to high latitudes. Consequently there is a stronger equatorward flux of PV and the vortex weakens. In between these extremes, days 40–60, there is typically less E–P flux convergence in the mid–upper stratosphere and an approximate balance holds between wave forcing and radiative relaxation. At this time there is a slight strengthening of the vortex under radiative effects before the E–P flux convergence increases and becomes the dominant influence. Since during the early and late phases the mean flow does not change enough to alter significantly the wave transmission properties, either the wave forcing or the radiative forcing, at a particular

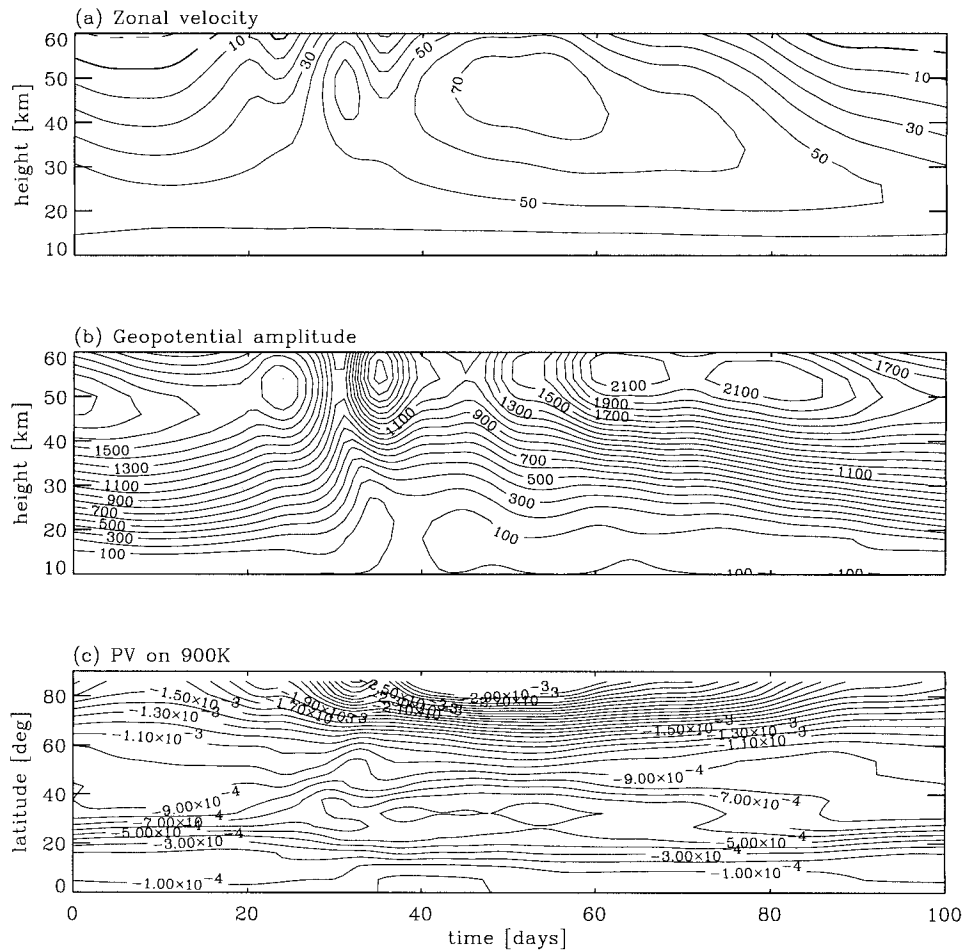
Vacillation v_2 , (N1, 140)

FIG. 5. Vacillation v_2 , obtained with radiative state N1 and wave forcing $h_0 = 140$. (a) Height–time cross section of zonal mean zonal velocity at 60° latitude, contour interval is 10 m s^{-1} ; (b) time–height cross section of wave-1 geopotential height amplitude, contour interval is 100 m ; (c) latitude–time cross section of PV on the 900 K isentropic surface (approximately 42 km), shading interval is $10^{-4} \text{ K kg}^{-1} \text{ m}^2 \text{ s}^{-1}$.

height or latitude, dominates for a prolonged period. It appears that radiative strengthening of the vortex in the early phase triggers a transition in the E–P flux, from a state in which the radiative forcing dominates to one in which the wave forcing dominates.

During the early, strengthening phase, days 20–35, there are two short events of more rapid deceleration accompanied by increases in the geopotential height amplitude. These events resemble minor stratospheric warmings. The E–P flux cross sections for the beginning of the second, occurring over days 29–33, are shown in Fig. 7. These show a region of strong flux convergence situated in the upper stratosphere around 30° latitude on day 29. This region then moves poleward as it rearranges the PV distribution, the strengthening of the PV gradients on the poleward flank of the region enabling stronger poleward wave propagation. Time–

height cross sections of the geopotential height phase (not shown) reveal an almost barotropic structure in the mid–upper stratosphere that propagates eastward with a phase speed roughly equivalent to a displacement of 90° in 4 days.

d. Vacillation v_3

For still stronger forcing, with $h_0 \geq 150 \text{ m}$ (for N1), a qualitatively different vacillation type, v_3 , is obtained. Whereas in v_2 above, the evolution consisted of relatively small, gentle undulations of zonal mean quantities, in v_3 there is a phase of rapid deceleration that more closely resembles a major sudden warming with a reversal of the zonal velocities at high latitudes. The evolution in general remains further from radiative equilibrium, except for several days prior to the warming.

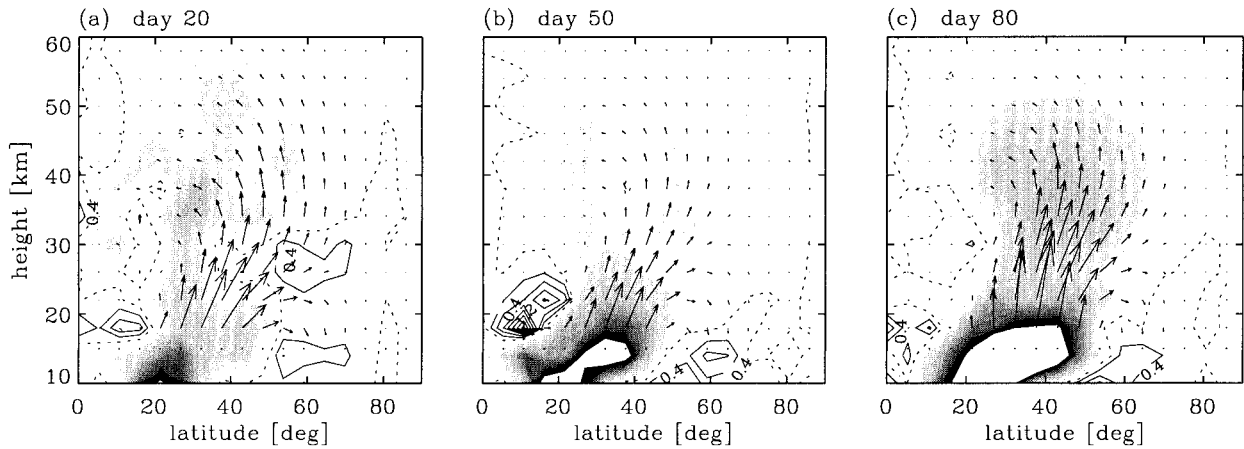
Vacillation v_2 , (N1. 140): EP cross-sections

FIG. 6. Vacillation v_2 , E-P flux, and divergence: (a) day 20; (b) day 50; (c) day 80. Contour and shading interval is 0.4 in the units of Fig. 3.

With the D radiative state the transition from v_2 to v_3 is complicated by a range of h_0 that yields intermittent responses with signals of both vacillations. With the N1 radiative state, however, there is a more definite transition from v_2 to v_3 between $h_0 = 145$ and $h_0 = 150$. Here, the only sign of a mixed response appears for $h_0 = 150$ in which case the first 1000 days is dominated by v_2 after which time v_3 is established. For $h_0 = 160$ the response is purely v_3 with a period of approximately 100 days. This period decreases as the forcing is increased further, though the main characteristic, the sudden warming, remains. For $h_0 = 200$ m the period is approximately 65 days; this case is examined in detail now.

The time evolution of zonal mean velocity, geopotential height amplitude, and zonal mean potential vorticity over a typical vacillation cycle (taken from days 870–970 of N1 with $h_0 = 200$, relabeled as days 0–100) is shown in Fig. 8. There are clear differences between this vacillation and the previous vacillation, v_2 , discussed above. The zonal wind Fig. 8a undergoes a gradual acceleration over days 0–45, followed by a rapid deceleration over days 45–49, during which time the strong westerlies reverse to easterlies throughout the mid- and upper stratosphere in mid- and high latitudes. These easterlies persist for the remainder of the cycle until around day 70 (regarding day 0 as the beginning of the cycle). During the rapid deceleration stage the

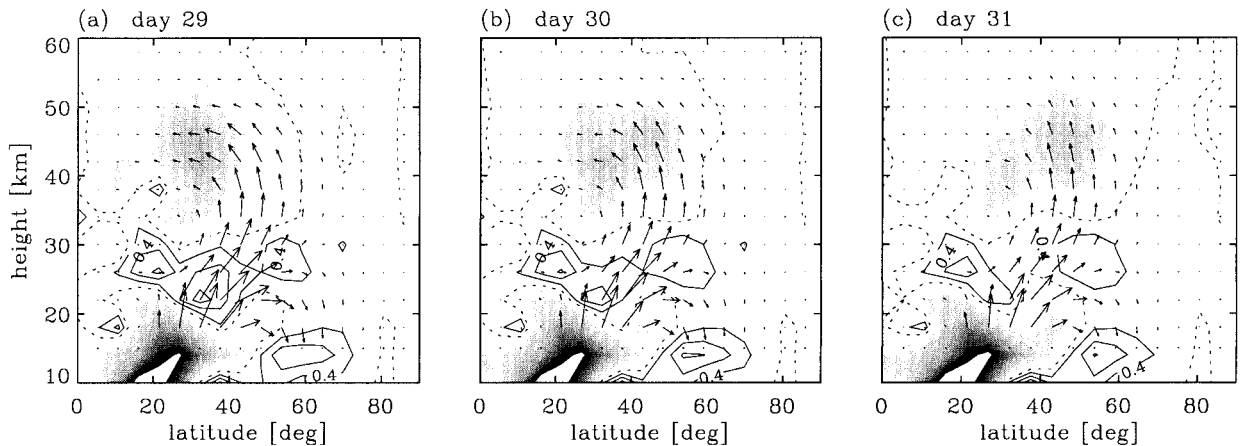
Vacillation v_2 , (N1. 140): EP cross-sections

FIG. 7. Vacillation v_2 , E-P flux, and divergence: (a) day 29; (b) day 30; (c) day 31. Contour and shading interval is 0.4 in the units of Fig. 3.

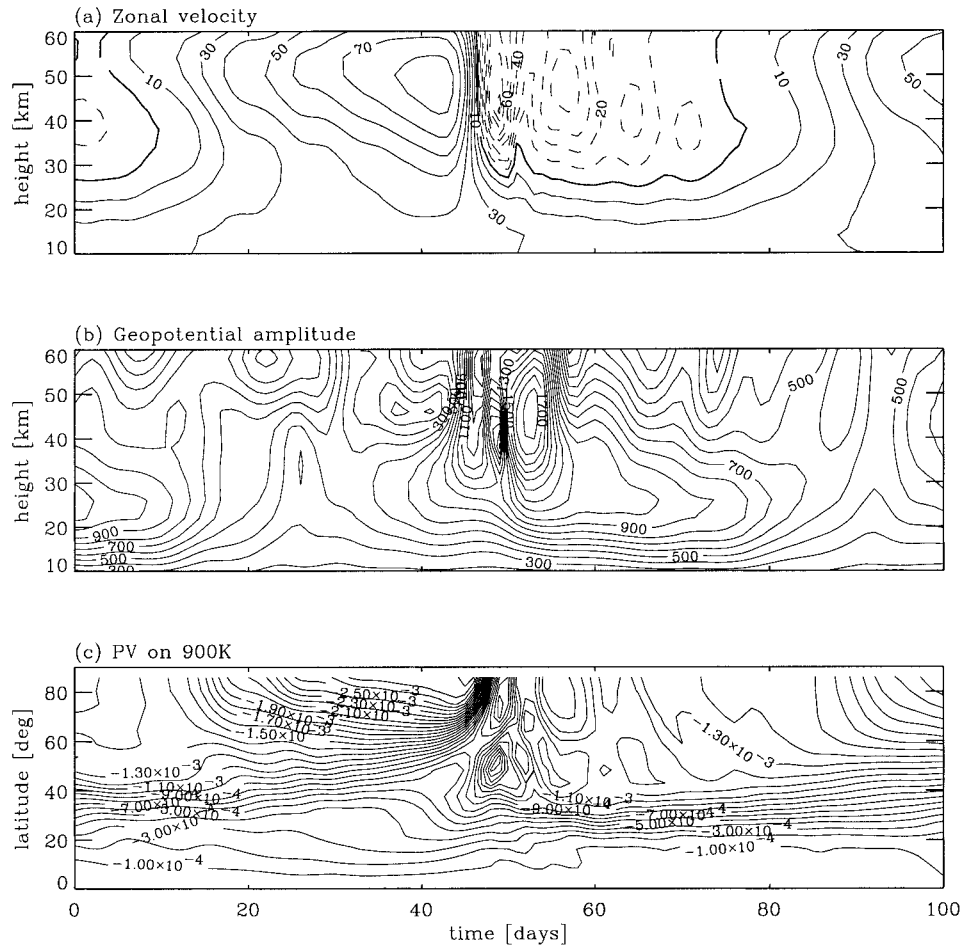
Vacillation v_3 , (N1, 200)

FIG. 8. Vacillation v_3 , obtained with radiative state N1 and wave forcing $h_0 = 200$. (a) Height–time cross section of zonal mean zonal velocity at 60° latitude, contour interval is 10 m s^{-1} ; (b) time–height cross section of wave-1 geopotential height amplitude, contour interval is 100 m; (c) latitude–time cross section of PV on the 900-K isentropic surface (approximately 42 km), shading interval is $10^{-4} \text{ K kg}^{-1} \text{ m}^2 \text{ s}^{-1}$.

geopotential wave amplitude increases rapidly to larger values than are present in other stages of the cycle. Immediately after the rapid deceleration the flow is highly disturbed and there is considerable variability of the easterlies. Then wave effects diminish and the flow begins to accelerate again under the effects of radiative relaxation.

The meridional structure of the zonal velocity also changes significantly during the v_3 vacillation cycle (Fig. 9), compared with the relatively small changes in v_2 above. After the easterlies have given way to westerlies during the gradual acceleration stage, there is a small but systematic variation with time of the meridional structure (days 10–40) as the vortex intensifies and moves poleward. After day 40, a region of low-latitude easterlies appears in the mid- and upper stratosphere, intensifies, and moves poleward. As this region gradually moves into midlatitudes the polar vortex also

tightens further, until by day 46 there is a strong, tight vortex confined to high latitudes, Fig. 9d. Figure 8c shows how the PV gradient strengthens significantly over days 40–46. From day 47 the region of midlatitude easterlies continues to intensify and move poleward, until by day 50 it has displaced the polar vortex and the entire zonal flow in the mid- and upper stratosphere in mid- and high latitudes is easterly. The zonal flow following this displacement remains transient for some time while large wave amplitudes remain. After around day 55 radiative effects begin to dominate wave effects and the zonal flow accelerates again.

The evolution can again be explained by consideration of E–P cross sections and PV gradients. During the early part of the vacillation cycle (days 0–30) the PV gradients throughout much of the stratosphere are weak and there is relatively little upward wave propagation. During this time the high-latitude mean flow

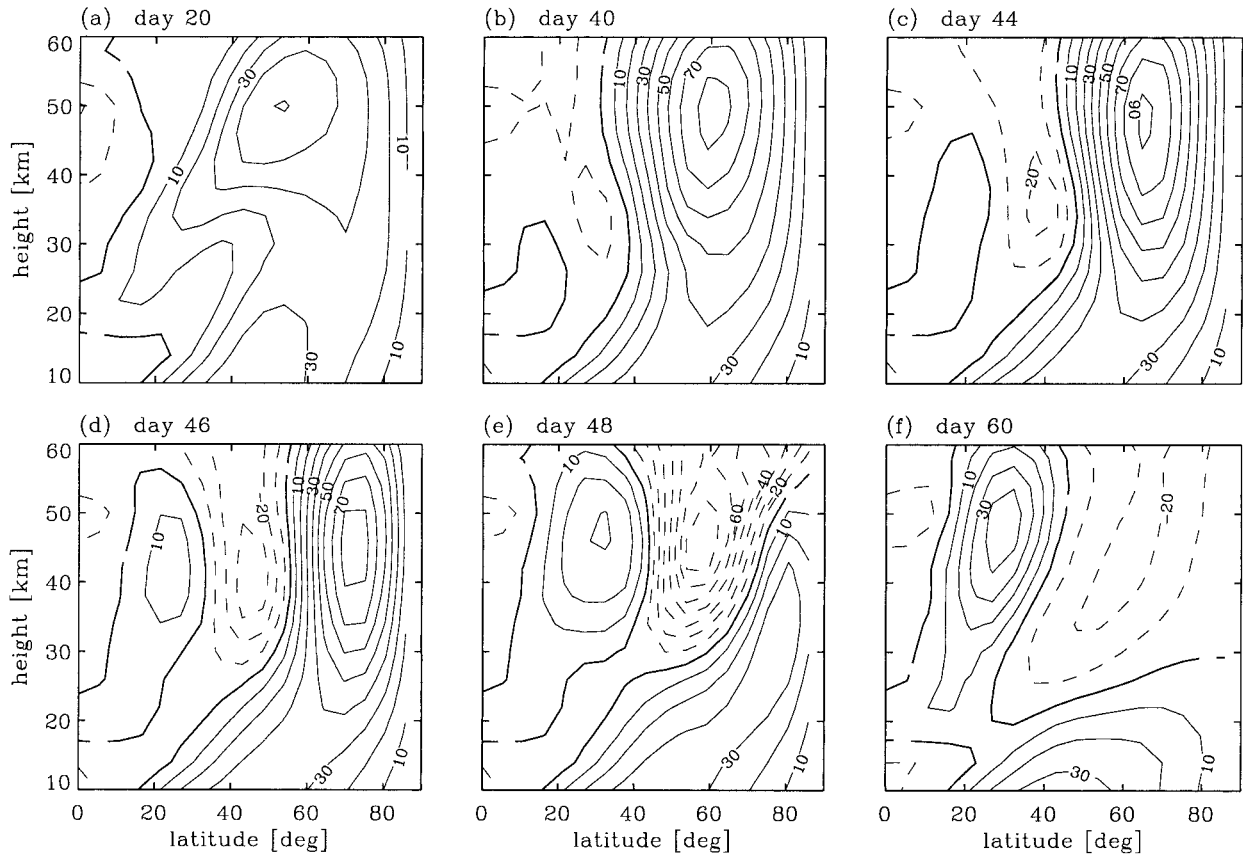
Vacillation v_3 , (N1, 200): zonal velocity

FIG. 9. Vacillation v_3 , height–latitude cross sections of zonal-mean zonal velocity: (a) day 20; (b) day 40; (c) day 44; (d) day 46; (e) day 48; (f) day 60. Contour interval is 10 m s^{-1} , solid lines are positive, dashed lines are negative, and thick lines are zero.

accelerates under radiative effects and wave-induced deceleration is confined to low latitudes. By day 40 the vortex and PV gradients have increased sufficiently to make upward wave propagation more favorable. There is then a feedback effect on the vortex; upward wave propagation gives rise to E–P flux convergence in mid-latitudes, which results in an equatorward flux of PV, strengthening the gradients to the north of the region of convergence, weakening those to the south. The adjusted PV gradients in turn favor wave propagation into higher latitudes. Thus the region of flux convergence, originally in midlatitudes on day 40, moves poleward as it rearranges the PV distribution and forms the strong, tight vortex confined to poleward of 60° ; see Fig. 10. By day 48, at which time the vortex is being destroyed, the main region of flux convergence is centered around 60° , and at these higher latitudes the convergence has a much stronger effect on the zonal mean velocities because of the smaller angular momentum here. Beyond day 48 the high-latitude westerlies have been replaced by easterlies, the strong PV gradients have been de-

stroyed, and further upward wave propagation is prevented.

Care is required when looking at such Eulerian mean diagnostics, since the wave amplitudes around the time of the rapid mean flow deceleration are large compared with the mean state itself. Thus the most likely explanation for such strong zonal mean easterlies at high latitudes is the displacement of the vortex from over the pole, at least within the constraints of a wave-1 truncated model. [Hsu (1981) discusses some of the limitations, in such situations, of models that include only zonal mean and wave 1.] This is seen from polar stereographic plots of the potential vorticity on the 750 K isentrope over days 44–48, shown in Fig. 11. But in addition to illustrating the displaced position of the vortex by day 46, the sequence also shows the rapid shrinking of the vortex and tightening of the PV gradient at high latitudes.

The low- to midlatitude vortex erosion and high-latitude intensification of PV gradients is present in both v_2 and v_3 vacillation types in the early, acceleration

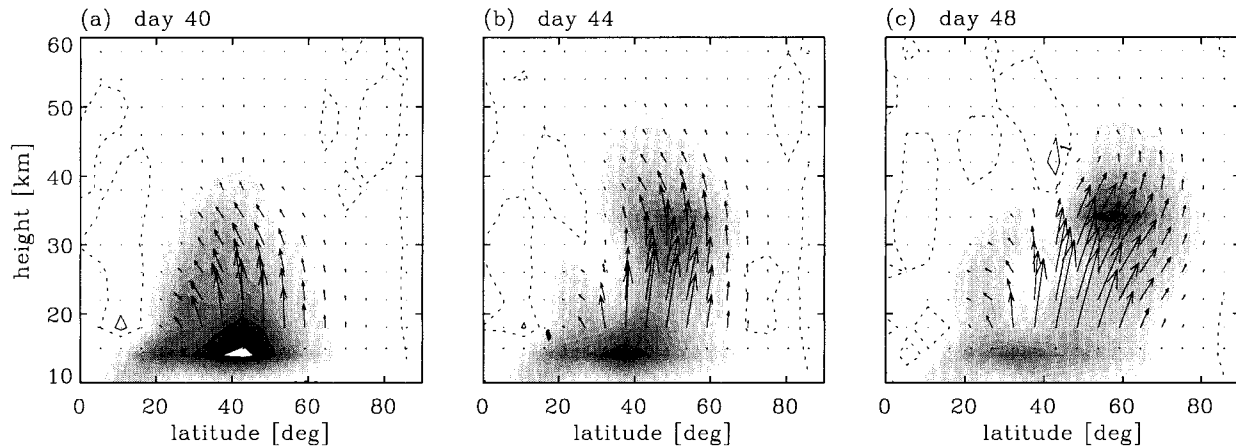
Vacillation v_3 , (N1. 200): EP cross-sections

FIG. 10. Vacillation v_3 , E-P flux, and divergence: (a) day 40; (b) day 44; (c) day 48. Contour and shading interval is 0.4 in the units of Fig. 3.

stages of the cycles. Such evolution is similar to the preconditioning that has been identified in sudden warming studies by, for example, Dunkerton et al. (1981) and Hsu (1981). The preconditioning is, however, much stronger in v_3 and only in this case do the high-latitude gradients become large enough to enable significant poleward focusing of waves and the subsequent rapid vortex destruction.

4. Further remarks

a. Comparison with lower-dimensional model results

Since the aim of this study is to extend the work of Yoden (1987a,b) on vacillating responses of a height-dependent channel model to a model with both height and latitude structure, it is appropriate now to compare the responses obtained in the two models. The previous section discussed two steady states, s_0 and s_1 , and two

vacillating states, v_2 and v_3 , in the model with height and latitude structure. Yoden also found two steady states and two vacillating states, which we shall denote by ys_0 , ys_1 , yv_2 , yv_3 , respectively, occurring in this order for increasing values of wave forcing. The bifurcation diagram for these four responses as a function of the forcing parameter, yh_0 , is different from that of this study implied by Table 1. As in our case, Yoden found responses ys_0 and ys_1 to exist for identical values of yh_0 , but in his case ys_1 lost stability earlier giving way to yv_2 through a Hopf bifurcation. Thus there was a range of forcing values that had ys_0 and yv_2 as possible multiple responses.

Despite some differences between the two vacillation responses of Yoden, yv_2 and yv_3 , both relied on low-level easterlies to prevent upward wave propagation during a dynamically inactive stage of each vacillation cycle. During this dynamically inactive stage the upper-

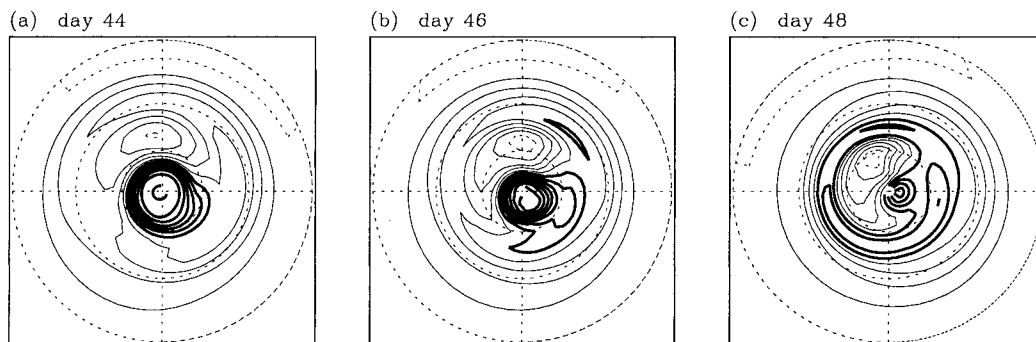
Vacillation v_3 , (N1. 200): PV on 750K isentrope

FIG. 11. Vacillation v_3 , PV on the 750 K isentropic surface (approximately 38 km): (a) day 44; (b) day 46; (c) day 48. Contour interval is $10^{-4} \text{ K kg}^{-1} \text{ m}^2 \text{ s}^{-1}$, thick lines are values $\geq 5 \times 10^{-4}$, dotted lines are zero, concentric dotted circles are 0° , 30° , 60° latitude circles.

level westerlies strengthened under radiative effects and when the low-level easterlies ceased the upward wave propagation led to a strong deceleration of the westerlies. In γv_2 this deceleration was more dramatic than that in γv_3 despite the stronger wave forcing in γv_3 . In comparison with v_2 and v_3 of the present study, there is most similarity between γv_2 and v_3 . Both rely on low-level easterlies to prevent upward wave propagation. One important difference that results from the extra latitudinal structure in v_3 is that after the easterlies cease the mean flow structure is still not favorable for upward and poleward wave propagation. In the v_3 case, therefore, the mean flow evolution remains dominated by radiative effects until much later. We also note that there is no counterpart of γv_3 , namely, a response to strong forcing that consists of only weak vacillations, in the study described here.

The steady-state responses of Yoden, ys_0 and ys_1 , also exhibited different vertical structure; ys_0 was close to radiative equilibrium, with strong westerlies that prevented upward wave propagation; ys_1 had a vertical structure consisting of two wave maxima and with waves of different phase in two separate regions. Between the two regions of ys_1 there is rapid change of phase tilt with height and stronger E–P flux convergence. In the current study the main difference between the two steady states, s_0 and s_1 , appears also in the E–P flux cross sections. Both show equatorward wave propagation but reflection to high latitudes is stronger in s_1 than in s_0 (see Figs. 3 and 4), resulting in a mean flow structure that is farther from radiative equilibrium.

It was claimed in Scott (1996) that s_1 did not exist in the current model as a result of the extra latitudinal structure. In that study a vacillating response, v_1 , was obtained instead because of reasons discussed in section 4c below. In fact the two steady states can exist for the same forcing value, with the different wave propagation patterns mentioned in the previous paragraph. Thus there is a correspondence between the two height-only steady states ys_0 and ys_1 and the two height–latitude steady states s_0 and s_1 .

b. Intermittent vacillation regimes

As described in sections 3c,d above the transitions between s_1 and v_2 and between v_2 and v_3 contain additional complicated dynamical regimes. In particular, the transition between v_2 and v_3 exhibits an intermittent regime, which contains signals of both the vacillating regimes in different time intervals. The intermittent regime was, however, less marked in the case of N1, from which s_0 , s_1 , v_2 , v_3 , above were taken, than in the case of D. For illustration the evolution of D over 10 000 days for selected values of h_0 between v_2 and v_3 are shown in Fig. 12.

The most striking picture of intermittence, albeit temporary, is obtained with $h_0 = 120$, shown in Fig. 12a by the zonal velocity at 60° latitude and 42-km height.

In the first half of the integration, up to day 5000, there are clearly discernable intervals of around 500 days during which v_2 is dominant, separated by intervals during which more dramatic, v_3 -like behavior, is dominant. What is perhaps most surprising is that after a time as long as 5000 days of apparently chaotic behavior, the evolution finally, or apparently finally, selects a single regime. A possible explanation might come from an examination of very low latitudes where effects of radiative relaxation are small; there may be a tendency for the v_3 -like disturbances to exert a small but systematic influence on the low-latitude zonal velocities toward a configuration more favorable to a sustainable v_2 regime. Such an explanation is speculative, but that low-latitude effects of this kind might be important in other systems has already been suggested by Scott and Haynes (1998) and by studies of the effects of the phase of the quasi-biennial oscillation on the high-latitude evolution (e.g., Holton and Tan 1982; Dunkerton and Baldwin 1991; O’Sullivan and Dunkerton 1994).

For larger forcing values, the intermittence is less clearly defined, but nevertheless present up to values around $h_0 = 150$. As expected, as the forcing is increased the time spent in a v_3 -like regime is also increased. As an example, the evolution for $h_0 = 140$ is shown in Fig. 12b and exhibits significantly more intervals during which the zonal velocity reverses to easterly. Similarly, intervals with v_2 -like behavior are fewer. However, the regime is still quite different from the pure v_3 regime, shown for $h_0 = 180$ in Fig. 12c for comparison.

c. Instability to latitudinally asymmetric disturbances

As stated in section 3 the steady-state regime, s_1 , obtained here under conditions of latitudinal symmetry, that is, on a hemisphere with a rigid boundary at the equator, is unstable to latitudinally asymmetric disturbances. Such disturbances were originally introduced into the model evolution by numerical round-off errors in the spectral transform routines. The final regime is a vacillating regime, denoted here by v_1 , that is quasi-periodic with a period of around 20 days and with an amplitude less than that of v_2 or v_3 (as measured by the zonal velocity at, say, 60° latitude and 38-km height). Although the amplitude of v_1 is less than that of v_2 , because of the much shorter period the deceleration stage of v_1 is more dramatic than that of v_2 , occurring over a time interval of around 4 days. Thus the v_1 regime resembles more closely a sequence of minor warmings.

From a mechanistic viewpoint, v_1 can also be understood in terms of E–P flux convergence and the rearrangement of potential vorticity. During the stage of the vacillation prior to the rapid mean flow deceleration the evolution of v_1 resembles that of v_3 ; vortex preconditioning occurs until poleward wave propagation is strong enough to induce rapid mean flow deceleration. The main difference is that whereas the stratospheric

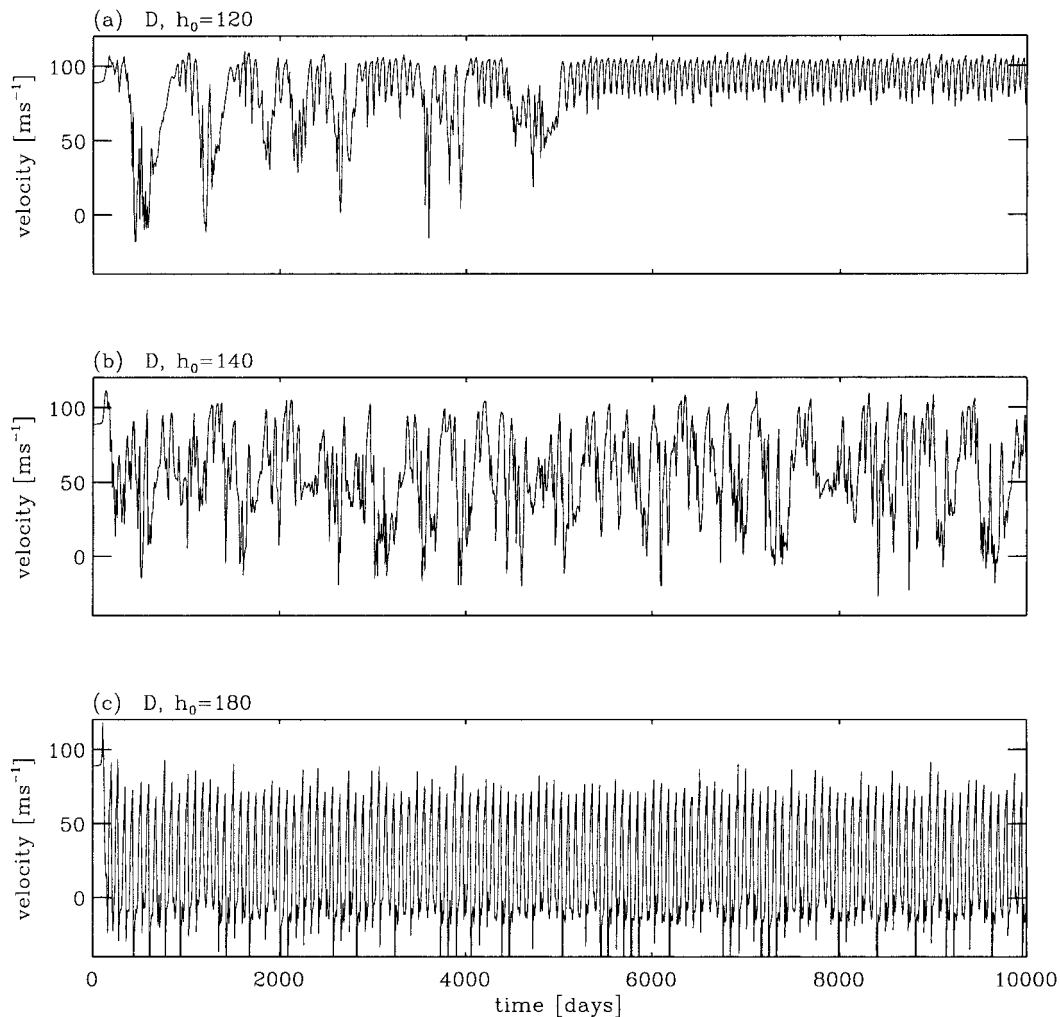
Intermittence v_2/v_3 , (D. 120–180)

FIG. 12. Time evolution of the zonal velocity at 60° latitude and 42 km height using the D radiative state and three different wave-forcing amplitudes: (a) $h_0 = 120$; (b) $h_0 = 140$; (c) $h_0 = 180$.

zonal mean velocities reverse to easterlies in v_3 , they do not in v_1 . In the early stages of the cycle, when the vortex is strengthening, waves are defocused to low latitudes. As midlatitude PV gradients increase, stronger wave flux into midlatitudes contributes to midlatitude PV rearrangement, resulting in stronger PV gradients to the north of the wave flux convergence, weaker gradients to the south. This rearrangement of PV gradients then allows for more wave propagation into higher latitudes. Eventually the waves propagate into sufficiently high latitudes and the rapid deceleration of the vortex occurs.

In accordance with the latitudinally asymmetric nature of the vacillation, the cycles in opposite hemispheres are in antiphase. Since there is no vacillation when latitudinal symmetry is enforced, it is likely that information of the evolution in one hemisphere is prop-

agated across the equator and influences the evolution of the opposite hemisphere. For example, there is some cross-equator zonal mean latitudinal velocity in the form of inertial instabilities that has peaks in magnitude at the same frequency as the vacillation. However, the strength of the peaks ranges from small to moderate without any obvious correlation to the strength of the corresponding vacillation cycle. The cross-equator flow is therefore unlikely to be a direct cause of the vacillation.

A more likely cause is suggested by the cross-equator E-P fluxes, which show a more regularly vacillating evolution. The effect that these fluxes have on the zonal mean zonal velocity produces a vacillating evolution at very low latitudes, up to 10° , that is nearly in antiphase with the evolution at higher latitudes. Specifically, during the gradual acceleration of the zonal flow at mid-

to high latitudes there is a deceleration of the zonal flow at low latitudes, that is a deceleration to an anomalous easterly flow. The size of the low-latitude velocity swing is around 8–10 m s⁻¹. It is conceivable that such anomalous low-latitude easterlies could contribute to, or even initiate, the process of vortex preconditioning that leads ultimately to the rapid deceleration. Further, such reasoning could also explain why the v_1 vacillations are more dramatic than v_2 , despite the wave forcing amplitude h_0 being less for v_1 .

d. Instability and resonance

It is seen from Figs. 5c and 8c that there are stages in each vacillation during which the potential vorticity gradients on isentropic surfaces reverse. It is therefore natural to ask whether shear instability plays a role in the evolution of the vacillation cycles. To examine the stability of the mean flow at various stages in the evolution the same model was integrated in a pseudo-linear configuration. In this configuration the zonal mean flow was held stationary at the value on a particular day by setting to zero the tendencies of the zonal components of the prognostic variables. Further, the lower-boundary wave forcing was reduced to zero at the beginning of the integration so that growth of wave-1 components can only be attributed to possible instability of the mean flow. The growth of the wave-1 components gives the growth rates of any unstable mode for that day.

For the case of v_2 it turns out that the only significant growth rates occur between days 0–5 and days 90–100, that is, the stage at which the vortex is weakest. The growth rate has a maximum of around 16 day⁻¹, around day 95, so it is possible that the instability contributes to the slight weakening of the polar vortex seen in Figs. 5a,c. The structure of the instability however, consists of an elongated region of flux divergence centered on 35° latitude, 28-km height and which tilts poleward with height, combined with a region of E–P flux convergence centered on 34° latitude, 25-km height with the same vertical tilt. The main point is that most of the flux convergence is confined to southward of 60° latitude and therefore probably does not contribute significantly to the weakening of the vortex. For the case of v_3 the growth rates are always too small to play an important role in the evolution of the vacillation cycle, which is generally on a much shorter timescale than the v_2 vacillation.

Finally, for the case v_1 described in section 4c above, it was found that there was an unstable mode with a growth rate of around 4 day⁻¹ occurring just before the time of the rapid deceleration of the vortex. The structure of this mode was in agreement with the structure of the E–P flux cross sections from the same time, suggesting that the instability may be contributing to the deceleration. However, the growth rate is still too small to account totally for the deceleration and the mean flow changes significantly over a similar timescale. It is

thought therefore that the effect of vortex erosion and the focusing of progressively more wave activity into higher latitudes remains the main factor.

A similar procedure was used to test for the possibility of resonance-like interaction between the mean flow and the lower-boundary wave forcing. Similar integrations to those described above were made except that the wave forcing was not reduced to zero but held at its original value. A linear increase with time of the latitudinally averaged vertical component of E–P flux through the lower boundary is suggestive of near-resonant behavior. Attention was given to the stages of the vacillations around the time of rapid vortex deceleration. No such linear growth of vertical E–P flux was found and it appears therefore that resonant-like behavior is not a significant factor in the vacillations.

5. Conclusions

A two-dimensional latitude–height primitive equation model with zonal and wave-1 longitudinal resolution has been used to investigate the possibility of steady and vacillating flow regimes obtained with constant external conditions. The strength of the imposed lower-boundary wave forcing and the “strength” of the radiative basic state are varied as external parameters between integrations, the latter being defined as the radiative state corresponding to a particular time in winter of the annual seasonal cycle. Integrations were run until a steady state was reached or else a vacillating state that appeared to be permanently established. Two qualitatively different steady states and two qualitatively different vacillating regimes were obtained and examined in detail for different wave-forcing amplitudes and the radiative state corresponding to late November.

One of the important discoveries is that the two different steady-state regimes were both obtainable under identical external conditions. That is, the model exhibited the possibility of multiple-flow equilibria previously only obtained in height-only models of the type studied by Yoden (1987a,b). Despite the possibility of multiple-flow equilibria, and therefore the possibility of rapid transitions between them, such a transition does not appear to be a likely candidate as a mechanism of stratospheric sudden warmings; for, at least in this study, the equilibrium states are relatively close together, and transitions between the two seem unlikely to be able to provide reductions of polar vortex strength comparable to those found in sudden warmings. However, the possibility of multiple equilibria is still an interesting property of the latitudinally dependent model. It arises here because of the different wave transmission properties associated with different meridional zonal mean flow structures. By contrast, the latitudinal degree of freedom was unavailable in the height-only channel model and consequently the results obtained in those studies are less directly comparable with processes in the real stratosphere.

Further interesting dynamical behavior was found in the vacillating regimes obtained with stronger wave-forcing amplitudes. Again the latitudinal freedom admitted different classes of vacillating regimes from those obtained with the height-only model. For moderate forcing values the response was small undulations of the mean flow, which remained westerly throughout the stratosphere for the duration of the vacillation cycle. For stronger forcing values the response was a rapid deceleration of the mean flow and reversal to easterlies, followed by a gradual acceleration of the mean flow. Both “weak” and “strong” vacillation regimes illustrated the importance of the meridional structure of the zonal mean flow in determining fluxes of wave activity and consequently in determining the mean flow evolution. By contrast, the vacillations obtained with height-only models ultimately relied on low-level easterlies to prevent the upward propagation of wave activity.

In between the extremes of the weak and strong vacillations, flow regimes were identified that contained signatures of both vacillations. These suggest a sensitivity of the response to the meridional structure of the mean flow. In particular, the response to radiative state D with forcing amplitude $h_0 = 120$ m, shown in Fig. 12a, which attains its final vacillating regime after around 5000 days, suggests that there is a small, systematic change of the meridional structure into a configuration for which this vacillating regime is stable.

A robust feature that appeared in both vacillation regimes discussed in section 3, as well as in a shorter vacillation regime obtained only when the condition of exact latitudinal symmetry was relaxed, discussed in section 4c, was the positive feedback of vortex erosion on the propagation and poleward focusing of wave activity. This feedback mechanism was always found to be responsible for the more rapid deceleration of the polar vortex during the vacillation cycles. It consists of a region of Eliassen–Palm flux convergence that rearranges the background potential vorticity gradient, and therefore changes also the wave propagation characteristics of the mean flow with a resulting poleward shift of the region of convergence. Clearly such a mechanism is missing in height-only models; its demonstration here is a step toward understanding internal variability in more complicated and realistic stratospheric models. One obvious extension of this work will be the inclusion of more zonal wavenumbers or of isotropic horizontal resolution.

Another issue is whether evidence of vacillating or (quasi-) steady states exists in model integrations that include a seasonally varying radiative basic state. Vacillations would need to be on a shorter timescale than that of the seasonal cycle. A related study (Scott 1996, chapter 3) has shown evidence of large wintertime vacillations at relatively large wave-forcing amplitudes compared with quiescent behavior, in which the zonal velocity follows the radiative basic state, at relatively

small wave-forcing amplitudes. Further dependence of the final state on the history of the wave-forcing amplitude suggested the possibility of multiple quasi-equilibria. A detailed investigation of the dependence of final state on radiative state, might consider a single wave-forcing amplitude, and a set of integrations with different, constant radiative basic states. Table 1 gives a first indication of what results might be found: for example, for $h_0 = 100$ the final state changes from s_1 to v_2 as the radiative basic state moves toward midwinter conditions; or for $h_0 = 140$ the final state moves from v_3 to v_2 to i .

Acknowledgments. We are grateful to two anonymous referees for helpful comments on the paper. Financial support for this work was provided by the U.K. Natural Environment Research Council and the U.K. Meteorological Office through a CASE studentship. The work of the Centre for Atmospheric Science is supported by the U.K. Natural Environment Research Council, in part through the U.K. Universities Global Atmospheric Modelling Programme, and by the Isaac Newton Trust. RKS is currently supported through the U.S. Office of Naval Research Grant N00014-98-1-0043.

REFERENCES

- Andrews, D. G., J. R. Holton, and C. B. Leovy, 1987: *Middle Atmosphere Dynamics*. Academic Press, 489 pp.
- Chao, W. C., 1985: Sudden stratospheric warmings as catastrophes. *J. Atmos. Sci.*, **42**, 1631–1646.
- Dunkerton, T. J., and M. P. Baldwin, 1991: Quasi-biennial modulation of planetary-wave fluxes in the Northern Hemisphere winter. *J. Atmos. Sci.*, **48**, 1043–1061.
- , C.-P. F. Hsu, and M. E. McIntyre, 1981: Some Eulerian and Lagrangian diagnostics for a model stratospheric warming. *J. Atmos. Sci.*, **38**, 819–843.
- Haltiner, G. J., and R. T. Williams, 1980: *Numerical Prediction and Dynamic Meteorology*. Wiley and Sons, 477 pp.
- Haynes, P. H., 1998: The latitudinal structure of the quasi-biennial oscillation. *Quart. J. Roy. Meteor. Soc.*, **124**, 2645–2670.
- , and M. E. McIntyre, 1987: On the representation of translating Rossby-wave critical layers and wave breaking in zonally truncated model. *J. Atmos. Sci.*, **44**, 2359–2382.
- Holton, J. R., 1976: A semi-spectral numerical model for wave, mean-flow interactions in the stratosphere: Application to sudden stratospheric warmings. *J. Atmos. Sci.*, **33**, 1639–1649.
- , and C. Mass, 1976: Stratospheric vacillation cycles. *J. Atmos. Sci.*, **33**, 2218–2225.
- , and H. C. Tan, 1982: The quasi-biennial oscillation in the Northern Hemisphere lower stratosphere. *J. Meteor. Soc. Japan*, **60**, 140–148.
- , P. H. Haynes, M. E. McIntyre, A. R. Douglass, R. B. Rood, and L. Pfister, 1995: Stratosphere–troposphere exchange. *Rev. Geophys.*, **33**, 403–439.
- Hoskins, B. J., and A. J. Simmons, 1975: A multi-layer spectral model and the semi-implicit method. *Quart. J. Roy. Meteor. Soc.*, **101**, 637–655.
- Hsu, C.-P. F., 1981: A numerical study of the role of wave–wave interactions during sudden stratospheric warmings. *J. Atmos. Sci.*, **38**, 189–214.
- Karoly, D., and B. J. Hoskins, 1982: Three dimensional propagation of planetary waves. *J. Meteor. Soc. Japan*, **60**, 109–123.
- Lait, L. R., 1994: An alternative form for potential vorticity. *J. Atmos. Sci.*, **51**, 1754–1759.

- Matsuno, T., 1970: Vertical propagation of stationary planetary waves in the winter Northern Hemisphere. *J. Atmos. Sci.*, **27**, 871–883.
- , 1971: A dynamical model of the stratospheric sudden warming. *J. Atmos. Sci.*, **28**, 1479–1494.
- McIntyre, M. E., 1982: How well do we understand the dynamics of stratospheric warmings? *J. Meteor. Soc. Japan*, **60**, 37–65.
- O’Sullivan, D., and T. J. Dunkerton, 1994: Seasonal development of the extratropical QBO in a numerical model of the middle atmosphere. *J. Atmos. Sci.*, **51**, 3706–3721.
- Scott, R. K., 1996: Seasonal and interannual variations of the stratospheric circulation. Ph.D. thesis, University of Cambridge, United Kingdom, 213 pp. [Available from Cambridge University Library, West Road, Cambridge CB3 9DR, United Kingdom.]
- , and P. H. Haynes, 1998: Interannual variability of the extratropical stratospheric circulation: The low-latitude flywheel. *Quart. J. Roy. Meteor. Soc.*, **124**, 2149–2173.
- Simmons, A. J., 1974: Planetary-scale disturbances in the polar winter stratosphere. *Quart. J. Roy. Meteor. Soc.*, **100**, 76–108.
- Yoden, S., 1987a: Bifurcation properties of a stratospheric vacillation model. *J. Atmos. Sci.*, **44**, 1723–1733.
- , 1987b: Dynamical aspects of stratospheric vacillations in a highly truncated model. *J. Atmos. Sci.*, **44**, 3683–3695.